UC San Diego

UC San Diego Previously Published Works

Title

Control of Unsaturation in De Novo Fatty Acid Biosynthesis by FabA

Permalink

https://escholarship.org/uc/item/4ww3w23p

Journal

Biochemistry, 61(7)

ISSN

0006-2960

Authors

Bartholow, Thomas G
Sztain, Terra
Young, Megan A
et al.

Publication Date

2022-04-05

DOI

10.1021/acs.biochem.2c00094

Peer reviewed

eScholarship.org Powered by the California Digital Library
University of California

Author Manuscript

Author Manuscript

Author Manuscript

Author Manuscript

HHS Public Access

Author manuscript

Biochemistry. Author manuscript; available in PMC 2023 April 05.

Published in final edited form as:

Biochemistry. 2022 April 05; 61(7): 608–615. doi:10.1021/acs.biochem.2c00094.

Control of unsaturation in *de novo* fatty acid biosynthesis by FabA

Thomas G. Bartholow[1], **Terra Sztain**[1], **Megan A Young**[1], **D. John Lee**[1,3], **Tony D. Davis**[1], **Ruben Abagyan**[2], **Michael D. Burkart**[1,*]

[1]Department of Chemistry and Biochemistry, University of California, San Diego, La Jolla, CA 92093-0340.

[2]School of Pharmacy and Pharmaceutical Sciences, University of California San Diego, La Jolla, CA, 92093, USA.

[3]Current address: Bioengineering and Therapeutic Sciences, University of California, San Francisco.

Abstract

Carrier protein dependent biosynthesis provides a thiotemplated format for the production of natural products. Within these pathways, many reactions display exquisite substrate selectivity, a regulatory framework proposed to be controlled by protein-protein interactions (PPIs). In *Escherichia coli*, unsaturated fatty acids are generated within the *de novo* fatty acid synthase by a chain length-specific interaction between the acyl carrier protein AcpP and the isomerizing dehydratase FabA. To evaluate PPI-based control of reactivity, interactions of FabA with AcpP bearing multiple sequestered substrates were analyzed through NMR titration and guided high-resolution docking. Through a combination of quantitative binding constants, residue-specific perturbation analysis, and high-resolution docking, a model for substrate control via PPIs has been developed. The *in silico* results illuminate the mechanism of FabA substrate selectivity and provide a structural rationale with atomic detail. Helix III positioning in AcpP communicates sequestered chain length identity recognized by FabA, demonstrating a powerful strategy to regulate activity by allosteric control. These studies broadly illuminate carrier protein dependent pathways and offer an important consideration for future inhibitor design and pathway engineering.

Graphical Abstract

[*]**Corresponding Author: Michael D. Burkart**, mburkart@ucsd.edu Department of Chemistry and Biochemistry, University of California, San Diego, Pacific Hall 6100D, 9500 Gilman Dr., La Jolla, CA 92093.

Author Contributions

Author Contributions: T.B. performed NMR experiments and Docking experiments. T.S. provided MD structures for docking. DJL provided NMR data and interpretation. M.A.Y. assisted protein preparation and analysis. TDD provided probes for chemoenzymatic loading. R.A. provided support and guidance. M.D.B. supervised the study and analysis.

Supporting information

A description of the experimental method, additional figures, and peak lists are available in the supplemental information.

Accession codes

The NMR data are available on the Biological Magnetic Research Bank under the ascension codes: 50699 and 50700. *E. coli* AcpP, UniProt entry P0A6A8; *E. coli* 3-hydroxydecanoyl-dehydratase FabA, Uniprot entry P0A6Q3.

Author Manuscript Author Manuscript Author Manuscript Author Manuscript

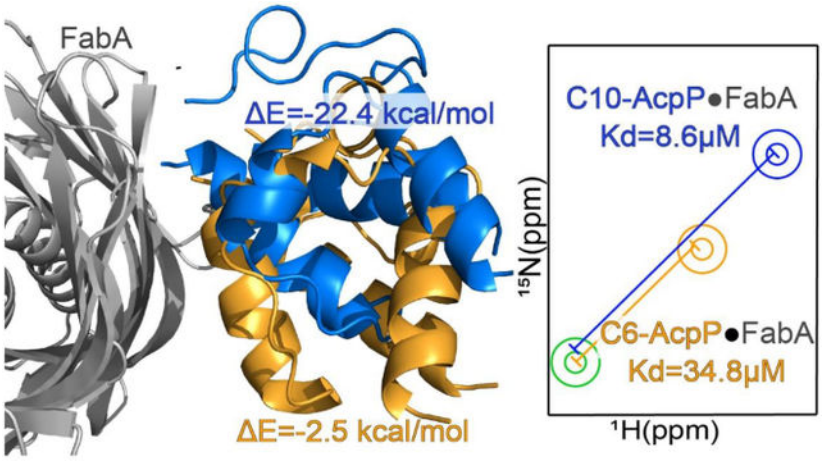

Keywords

Protein-protein interactions; Fatty acid biosynthesis; protein-protein docking; protein NMR

Introduction

Fatty acid biosynthesis (FAB), an essential primary metabolic pathway found across all domains of life, which produces not only the fatty acids required for membrane biogenesis and energy storage, is central to the biosynthesis of essential cofactors and cellular regulatory processes[1,2]. In *E. coli*, FAB exists as a precisely coordinated multi-enzyme pathway that must maintain control over both iterative and substrate-selective reactivity in order to maintain cellular homeostasis and environmental response[3–5]. This type II FAB expresses all of the protein components as stand-alone and freely diffusing enzymes/domains (Fig 1a), with *E. coli* FAB associated with more than 25 known participating enzymes[6–8]. Still, the membranes of *E. coli*, and by extension the resulting FAB products, are evolutionarily selected and dynamically tuned to the environment[9,10]. While the microbiological phenomena of fatty acid composition specificity have been observed[11,12], the molecular and enzymatic details of this control is just beginning to be unraveled. There remain multiple unknowns around how these enzymes can maintain selectivity over the dozens of possible substrates upon which they act to regulate such a complex and essential pathway.

An important mechanism may lie in the protein-protein interactions (PPIs) of the central FAB player, the acyl carrier protein (ACP), in its interactions with FAB enzymes[13,14]. The *E. coli* ACP, AcpP, is a small (~10 kDa), four-helical protein, with high homology to many other organisms' FAB systems. As such, AcpP has served as a model for other thiotemplated, or carrier protein-dependent, pathways[15,16].

Through each step, substrates that are covalently bound to the AcpP by a 4'-phosphopantheteine arm are accessed by partner enzymes through PPIs in order to elongate the cargo or perform tailoring reactions[17]. In FAB, elongation adds two carbon units to provide a β-ketone, which is fully reduced to the saturated alkane in three steps that involve

Author Manuscript Author Manuscript Author Manuscript Author Manuscript

formation of β-hydroxy and *trans*-α/β unsaturated intermediates. The *trans*-α/β unsaturated intermediate can undergo reduction to the fully reduced alkane. Alternatively, the *trans*-α/β-unsaturation can be isomerized to the *cis*-α/β-unsaturation and enter back into elongation in order to immortalize the *cis* double bond[18,19]. Throughout FAB elongation, ACP-bound intermediates can also be diverted to other enzymes to source fatty acids for the biosynthesis of molecules such as lipoic acid[20], acyl homoserine lactones[21], and lipid A[22].

ACPs carry the growing acyl chains covalently attached to a 4'-phosphopantetheine cofactor via a thioester linkage. The ACP has been found to sequester the acyl cargo inside of a hydrophobic pocket that is created by the four α-helices of the ACP structure (Fig 1b). Upon interaction with a partner enzyme, the cofactor and cargo are "chain-flipped" out of the pocket and into the active site of the partner enzyme[23,24]. After the reaction, the acyl chain is flipped back to sequester within ACP, thus protecting the substrate from hydrolysis. The PPI binding events have been previously demonstrated to occur rapidly, with the ACP and partner proteins forming transient interactions[25,26]. Published studies have demonstrated that substrate changes translate into structural modifications within the ACP, particularly upon helix III[27]. It has been thought that these structural changes effect partner enzyme interactions[28].

One of the most remarkable transformations within unsaturated FAB is the production of a C10:1 fatty acid. The first control step in unsaturation is catalyzed by 3-hydroxy-decanoyl dehydratase, FabA in *E. coli*. FabA's role in chain length-specific unsaturation has been established through both *in vitro* and metabolic flux experiments.[29,30] Specifically, FabA produces the C10:1 *cis* unsaturation by scavenging 3-hydroxy-decanoyl AcpP from the saturated FAB cycle (Fig 1a). For this, FabA performs a dual purpose. First, dehydrating to form *trans*-2-decenoate, then FabA performs an isomerization to *cis*-3-decenoyl AcpP. This substrate then continues to elongation by FabB. This process is the only entry to unsaturated fatty acids for *E. coli*. Previous studies have demonstrated that substrate analogs bearing a reactive chemical crosslinker loaded onto the AcpP will not react with partners when the probe does not mimic the natural ten-carbon substrate[31], suggesting a point of substrate control preceding full chain flipping into the partner active site (Fig 1B). The first crosslinked crystal structure of *E. coli* AcpP was reported of the AcpP=FabA complex (PDB: 4KEH) using crosslinking probes attached to AcpP in order to trap the active site histidine residue[26]. The crosslinked structure established the catalytic conformation of the AcpP=FabA complex, and associated NMR titration experiments demonstrated the ability to probe dynamic PPIs to understand pre-catalytic interactions.

FabA has a unique and important secondary role as an isomerase, isomerizing *trans*-2-decenoyl-AcpP into *cis*-3-decenoyl-AcpP[29,30]. We recently elucidated the mechanism and specificity of isomerization through comparison of the crosslinked structure with molecular dynamics (MD) analysis[32]. This reaction has been demonstrated to be highly selective, and we have reported that chemically reactive probes demonstrate specificity for C10 acyl chain lengths[31] We observed significant PPI-based substrate control by FabA using crosslinking probes that mimicked C6, C8, and C10- chain lengths tethered to AcpP[33]. The corresponding magnitude and specificity implicit in this interaction indicated that selectivity

Author Manuscript Author Manuscript Author Manuscript Author Manuscript

surpassed active site recognition and implicated a substrate-controlled PPI. This inspired us to study the phenomenon in more detail, beginning with solution-state NMR.

Here we report the evaluation of FabA chain length specificity through an analysis of AcpP structure bearing three acyl chain lengths: six, eight, and ten carbons. By uniting NMR titration analysis, MD minimized acyl-AcpP structures, and high-resolution protein docking, we evaluate the role of chain length to modify AcpP structure and the ability of those structural modifications to regulate FabA activity. This study presents a novel combination of structural and quantitative techniques to elucidate mechanisms of chain-length regulation in FAB.

Results

FabA titration with hexanoyl, octanoyl, and decanoyl AcpP

^{1}H-^{15}N HSQC NMR has found a role in the study of in solution interactions of AcpP with proteins[25,26], and we employed it here to observe the subtle differences in binding of the substrate bearing AcpPs with FabA. With the movement of peaks representing the average of the populations of states present in solution[34]. Uniformly labeled ^{15}N-AcpP was prepared and loaded with the three different probes with C6, C8, and C10 attached through aminopantetheine linkage[33]. These were titrated with increasing concentrations of unlabeled FabA to observe the residues which experienced peak migration upon ^{1}H-^{15}N HSQC NMR (Fig 2A). Saturated acyl chains were chosen as the tethered analogs to avoid reaction with FabA during experiments and remain consistent with prior crosslinking studies. However, future studies with catalytically inactive enzymes and the native substrate will be necessary to further study specificity.

The effect of the different chain lengths alone on the chemical shifts of AcpP led to the largest chemical shift perturbations (CSPs) at residues F28, D35, S36, E47, I54, D56, A59, I62, T64, and Q66 (Fig 2B, S1&2). These residues all reside along the hydrophobic pocket of AcpP, with many occurring at helix III or along the preceding loop. Across the three titrations we observed CSPs in similar regions of the AcpP (Fig 2C–E). The bulk of CSPs occurred in the helix II and III region and the helix II/III loop. However, the CSPs extended through the top of helix IV. Perturbation magnitude increased with each successive two-carbon increase in substrate size. From a mean CSP of 0.024 for C6, to 0.032 for C8, and 0.043 for C10 (Table 1).

The most perturbed residues of the C10-AcpP•FabA titration were located at D35, S36, D38, A45, E47, T52, I54, E57, A59, T63, Q66, and A68. The largest chemical shift differences between the C6 and C10-AcpPs alone correspond closely to these same most-perturbed residues in the titration with FabA. The most perturbed residues are neighboring or close to one another, except for F28, which remained one of the most perturbed residues. To compare the C6 and C10 titrations, the CSP values were normalized to the largest CSP within the data set (Fig S3). It was noted that CSPs unique to the C10-AcpP•FabA titration were I54, A59, T63, Q66, and A68, while the C6-AcpP•FabA titration had unique CSPs at residues L42, V43, V65, and Y71. Despite largely shared surface interactions, there are unique internal effects of FabA interacting with different cargo bearing AcpPs.

Author Manuscript Author Manuscript Author Manuscript Author Manuscript

Thermodynamic and kinetic parameters vary between AcpP substrates

TITAN line shape analysis was utilized to generate quantitative data from the NMR titrations performed[35]. Characterization of the titrations of C6 and C10-AcpP with FabA found that the C6-AcpP bound with 34.8 ± 5.9 μM affinity and 311 ± 64 s^{-1} off rate (Table 1, Fig S4). The C10-AcpP bound FabA with a 8.6 ± 3.0 μM Kd and 4535 ± 647 s^{-1} off rate. This demonstrates a significant effect upon increasing the chain length. It is compelling that an addition of four carbons in cargo size could affect such a significant change to the binding affinity. A structural rationale for this difference was sought further through high resolution docking.

AcpP•FabA 3D model

To evaluate these observations structurally, high-resolution docking was performed in the ICM fast fourier transform docking protocol using NMR titration data to guide the docking algorithm[36–39]. To ensure that the most relevant acyl-AcpP structure is used for docking, MD derived structures of AcpP with tethered acyl chains of differing chain lengths were docked with explicit acyl cargo (Fig 2F). Next, the partner FabA enzyme was prepared through solvation of the reported crystal structure (PDB: 1MKB)[40], optimizing the hydrogen bonding and angles to the water molecules. The interfaces of the AcpP are highly acidic, and those of FabA are basic (Fig 2G), making accurate preparation of structures for hydrogen bonding important to accurate modeling. FabA was docked to the three different MD derived structures using identical methodologies except for varying the beginning AcpP inputs. The structures were sorted based on their RMSD to the post-catalytic crosslinked crystal structure 4KEH, and the most thermodynamically favorable model within 5Å of the crosslinked structure was chosen for each chain length (Fig S6). This cutoff was chosen to accommodate the differences between a crosslinked complex and docked complex, both due to the unbound FabA and the un-chain flipped and precatalytic AcpP. Based on this analysis, we have noted that the energetics of the bound complexes agrees with the TITAN analysis and CSPs (Table 1). The AcpPs from the MD study were observed to vary most heavily and distinctly in the helix III region of AcpP (Fig 3a,b), matching the same regions identified by NMR titration studies above. Combined with the observation that the FabA interface is most heavily electropositive in the region which binds helix III, we identified an important role in recognition at helix III of AcpP.

Next it was examined whether the AcpPs would demonstrate different ability to bind FabA based on the docked thermodynamics. The energies of the three interactions were well in line with the known substrate preferences (Table 1), with C6 binding with an overall energy of −2.5 kcal/mol, C8 with an overall energy of −11.8 kcal/mol, and C10 with an overall energy of −22.4 kcal/mol[38]. These energies are not definitive alone, but they are useful for examining how well the AcpP conformations complement the surface of FabA. To appreciate exactly how these minor changes translate to differences in surface binding, we next examined the interface in detail, focusing on helix III.

Identifying structural features which facilitate specificity

To examine exactly which AcpP residues were most important to the interaction, the docked models were examined relative to one another (Fig 4, S4&7). There were several regions of

Author Manuscript Author Manuscript Author Manuscript Author Manuscript

the protein which were identified as important to the interactions, with the most significant occurring on helix III.

In the C10 docked structure, there appeared to be a coordinated network of interactions with three acidic residues, D56, E57, and E60, within a distance to form interactions with R136', the R137' backbone, and the R137' side chain, respectively. (Residues on FabA will be noted by a " ' " throughout the text.) These docked models likely represent a bound but non-chain-flipped encounter complex, representing an initial binding interaction. The C8 helix III structure demonstrates poorer binding, with helix III out of orientation and only one coordinated residue at E57 nearby R136'. E60 appears to be oriented such that there is no space for R137' to rotate and bind. C6 binds similarly, but with D56 successfully coordinating R136', reflecting how the orientation of helix III determines the creation of three critical interactions in C10. It appears that shorter chain lengths cannot form all three of these encounter complex interactions. Binding would require structural rearrangement and hinder rapid binding.

Two additional identified interactions lie on residues E41 and E47. E41 interacts with K161', and only C10 and C6 docked models, but not C8, are within approximate range (within ~3Å) to interact. E47 appears to be important in stabilizing the bottom of helix II, though it is out of interacting distance in the docked pose at 6Å, and it may interact upon full binding. Next, to complement these two studies, the CSP values were projected onto the docked AcpP structures (Fig 5). In addition to noting several strong internal perturbations, most significantly I54, two interactions were noted at D35 and D38. These residue bridges have been identified previously as participating in the stabilizing of the chain-flipped acyl chain[26]. However, it was noted that D35 was also within a proper hydrogen bonding distance to the backbone of A170'. These interactions may also anchor helix II, along with the important salt bridges identified at E41 and E47. This interaction would have been impossible to identify in the crosslinked structure, where the loop with A170 was not resolved in the crystal structure. I54 has been identified as involved in chain flipping by examining its distance from interactions and positioning of the side chain directly into the acyl pocket. We have additionally examined the docked models of C6 and C8-AcpP in the Supplemental Information.

Taken together, these data create a compelling picture of FabA's chain length selectivity as determined by the PPIs with C6, C8, and C10 acyl chain sequestered AcpP. The CSPs reflect different surface interactions from the crosslinked crystal structure, while the magnitude of the CSPs with increasing chain length is in agreement with the TITAN analysis. This demonstrates a mechanism of substrate-dependent selectivity and regulation based upon the substrate-induced structure of AcpP. Here, the unique positioning of helix III is dictated by the respective influence of sequestered chain lengths. These structural differences, though subtle, are significant enough that the most energetically stable docking poses appear to be occluded in shorter chain lengths. This conclusion is further supported by the corroborating thermodynamic and CSP data.

Author Manuscript Author Manuscript Author Manuscript Author Manuscript

Expanding analysis of FabA docked states

To explore the full structural space of FabA • AcpP interactions, docking was performed to observe secondary binding modes. Using the C6, C8, and C10 models examined above as reference structures, a second docking calculation was performed with all docked poses examined based on their RMSD to the minimized model. The docked states were then graphed by RMSD vs energy (Fig 5) to observe other potential binding modes. In the C10 binding, a cluster of low RMSD conformations (~5Å) were observed (Fig 5A), along with a second cluster of stable secondary states at higher RMSD (~15Å) (Fig 5E). A second, lower energy state, was also observed at ~13Å RMSD from the preliminary model (Fig 5F). This model has FabA adopting a similar docked site (Fig S5), but with the AcpP directed more sharply into the FabA face. In addition, multiple low energy, higher RMSD states sampled features of the FabA interface. The C8 docked data displayed that the model closest aligned to the crosslinked-like structure was higher energy than a set of ~7Å RMSD models (Fig 5B,S5). The lowest energy of these adopts a similar structure to the crosslinked-like model examined. Lastly, C6 showed few low energy states, and low RMSD to the crosslinked-like state. The lowest energy model occurred at ~17Å RMSD from the docked model examined above (Fig 5C,S5). However, this state, as well as multiple similar energy states, docked "upside-down," likely with no ability to perform a functional interaction that could result in chain-flipping.

Discussion

Evaluation of this data demonstrates several key concepts. First, the "active" cross-link-like conformation, which is stable in the C10-AcpP docked model, is less energetically favorable for shorter chain lengths. The C8-AcpP docked model was observed to have a small set of favorable structures which were relatively similar to the active model; and C6's were significantly different. This could explain the observation that FabA crosslinking experiments with C8 analogs were more favorable than with C6 variants[31], given that C8 can form more stable PPI conformations. Finally, it has been long known that the AcpP • partner enzyme interface is a dynamic interaction[26,32,41]. We predict that the various energetically favorable bound states can constitute encounter complexes[42,43], or preliminary interactions that bind the AcpP transiently and allow rearrangement of the AcpP into the active state. This PPI mechanism would eliminate the need for many transient binding events, allowing the AcpP to associate with the interface in order to form a catalytic interaction from more than just one perfectly aligned binding event with a partner enzyme.

These experiments demonstrate the role of the AcpP sequestered substrate in the PPI-controlled catalysis of FabA. Here, the identity of the substrate is pivotal to the positioning of helix III to attain favorable FabA binding. By merging our knowledge of the structural effects of chain length with observations of substrate specificity, we show how FabA, and presumably all other AcpP partner enzymes, maintain a control step over possible substrates tethered to AcpP before the chain flipping process commits the substrate into the active site. This PPI-based specificity mechanism has been hypothesized as an explanation for substrate specificity, although it had not been demonstrated for FabA[44]. While prior demonstration of selective crosslinking of FabA by a substrate-mimicking crosslinker favored C10-AcpP

Author Manuscript Author Manuscript Author Manuscript Author Manuscript

over C6 or C8[31,45], the phenomenon of substrate controlled PPI has not been specifically identified. This study presents a structural model for explaining this specificity, with additional work necessary to fully understand the mechanism. However, this can serve as a foundation to build the understanding of this phenomenon. This first step required leveraging dynamic studies by NMR to examine the solution interactions of acyl-AcpP with FabA, to inform docking simulations, and to provide confirmatory thermodynamics.

Further, we observe the formation of several stable conformations of the acyl-AcpP • FabA interaction that are near or in the path of the crosslinked conformation. These states around the catalytic structure of AcpP may present an expanded paradigm for AcpP • partner interactions that capture encounter complexes that form prior to the chain-flipping event. Stable secondary interfaces could help lead acyl-AcpP, which may initially bind non-ideally, to the active bound conformation required for chain-flipping. This explains the plasticity of the AcpP interface, with few studies identifying single mutations sufficient to abolish activity[46,47]. These findings also explain the remarkable efficiency of FAB, with the ability of acyl-AcpP to be “funneled” from improperly coordinated binding events into the required conformation.

Previous microbiological and biochemical studies have demonstrated the role of FabA in scavenging acyl-AcpP pools to perform unsaturation. This work now presents a model for a first control step, maintaining the essential specificity by PPIs evolved to selectively recognize C10-AcpP structure. Unsurprisingly, these findings required a highly interdisciplinary methodology that relied on a fusion of experimental and computational analyses. This model for rapidly sampled chain length specificity must certainly extend beyond FabA, and likely accounts for acyl chain selectivity across some of the 25 known AcpP-dependent enzymes in *E. coli*, explaining both the speed and precision evolved into FAB. We suspect that these phenomena are involved in all thiotemplated pathways that sequester intermediates within the carrier protein, providing a powerful and fundamental control mechanism.

Supplementary Material

Refer to Web version on PubMed Central for supplementary material.

ACKNOWLEDGMENT

We thank Stan Opella, Xuemei Huang, and the UCSD biomolecular NMR facility for support and guidance.

Funding Sources

This work was funded by NSF IOS-1516156 and NIH R01GM095970.

ABBREVIATIONS

ACP	Acyl carrier protein
AcpP	The *E. coli* carrier protein
FAB	Fatty acid biosynthesis

Author Manuscript Author Manuscript Author Manuscript Author Manuscript

FabA	The E. coli isomerizing 3-hydroxydecanoyl dehydratase
HSQC	Heteronuclear single quantum coherence
NMR	Nuclear magnetic resonance spectroscopy
MD	molecular dynamics

REFERENCES

(1). Crosby J; Crump MP The Structural Role of the Carrier Protein – Active Controller or Passive Carrier. Nat. Prod. Rep 2012, 29 (10), 1111–1137. 10.1039/C2NP20062G. [PubMed: 22930263]

(2). Lai JR; Koglin A; Walsh CT Carrier Protein Structure and Recognition in Polyketide and Nonribosomal Peptide Biosynthesis. Biochemistry 2006, 45 (50), 14869–14879. 10.1021/bi061979p. [PubMed: 17154525]

(3). Tan Z; Black W; Yoon JM; Shanks JV; Jarboe LR Improving Escherichia Coli Membrane Integrity and Fatty Acid Production by Expression Tuning of FadL and OmpF. Microb. Cell Factories 2017, 16 (1), 38. 10.1186/s12934-017-0650-8.

(4). Shokri A; Larsson G Characterisation of the Escherichia Coli Membrane Structure and Function during Fedbatch Cultivation. Microb. Cell Factories 2004, 3, 9. 10.1186/1475-2859-3-9.

(5). Rock CO Opening a New Path to Lipoic Acid. J. Bacteriol 2009, 191 (22), 6782–6784. 10.1128/JB.01151-09. [PubMed: 19734307]

(6). Gully D; Moinier D; Loiseau L; Bouveret E New Partners of Acyl Carrier Protein Detected in Escherichia Coli by Tandem Affinity Purification. FEBS Lett. 2003, 548 (1–3), 90–96. 10.1016/s0014-5793(03)00746-4. [PubMed: 12885413]

(7). Lay NRD; Cronan JE In Vivo Functional Analyses of the Type II Acyl Carrier Proteins of Fatty Acid Biosynthesis. J. Biol. Chem 2007, 282 (28), 20319–20328. 10.1074/jbc.M703789200. [PubMed: 17522044]

(8). Gully D; Bouveret E A Protein Network for Phospholipid Synthesis Uncovered by a Variant of the Tandem Affinity Purification Method in Escherichia Coli. PROTEOMICS 2006, 6 (1), 282–293. 10.1002/pmic.200500115. [PubMed: 16294310]

(9). Cronan JE; Thomas J Bacterial Fatty Acid Synthesis and Its Relationships with Polyketide Synthetic Pathways. Methods Enzymol. 2009, 459, 395–433. 10.1016/S0076-6879(09)04617-5. [PubMed: 19362649]

(10). Magnuson K; Jackowski S; Rock CO; Cronan JE Regulation of Fatty Acid Biosynthesis in Escherichia Coli. Microbiol. Mol. Biol. Rev 1993, 57 (3), 522–542.

(11). Sohlenkamp C; Geiger O Bacterial Membrane Lipids: Diversity in Structures and Pathways. FEMS Microbiol. Rev 2016, 40 (1), 133–159. 10.1093/femsre/fuv008. [PubMed: 25862689]

(12). Rock CO; Jackowski S Incorporation and Turnover of Fatty Acids in Escherichia Coli Membrane Phospholipids. In Advances in Lipobiology; Gross RW, Ed.; JAI, 1996; Vol. 1, pp 39–59. 10.1016/S1874-5245(96)80004-8.

(13). Chan DI; Vogel HJ Current Understanding of Fatty Acid Biosynthesis and the Acyl Carrier Protein. Biochem. J 2010, 430 (1), 1–19. 10.1042/BJ20100462. [PubMed: 20662770]

(14). Finzel K; Lee DJ; Burkart MD Using Modern Tools to Probe the Structure-Function Relationship of Fatty Acid Synthases. Chembiochem Eur. J. Chem. Biol 2015, 16 (4), 528–547. 10.1002/cbic.201402578.

(15). Byers DM; Gong H Acyl Carrier Protein: Structure–Function Relationships in a Conserved Multifunctional Protein Family. Biochem. Cell Biol 2007, 85 (6), 649–662. 10.1139/O07-109. [PubMed: 18059524]

(16). Majerus PW; Alberts AW; Vagelos PR Acyl Carrier Protein, Iv. the Identification of 4′-Phosphopantetheine as the Prosthetic Group of the Acyl Carrier Protein. Proc. Natl. Acad. Sci 1965, 53 (2), 410–417. 10.1073/pnas.53.2.410. [PubMed: 14294075]

Author Manuscript Author Manuscript Author Manuscript Author Manuscript

(17). Cronan JE The Chain-Flipping Mechanism of ACP (Acyl Carrier Protein)-Dependent Enzymes Appears Universal. Biochem. J 2014, 460 (2), 157–163. 10.1042/BJ20140239. [PubMed: 24825445]

(18). Feng Y; Cronan JE Escherichia Coli Unsaturated Fatty Acid Synthesis. J. Biol. Chem 2009, 284 (43), 29526–29535. 10.1074/jbc.M109.023440. [PubMed: 19679654]

(19). Cao Y; Yang J; Xian M; Xu X; Liu W Increasing Unsaturated Fatty Acid Contents in Escherichia Coli by Coexpression of Three Different Genes. Appl. Microbiol. Biotechnol 2010, 87 (1), 271–280. 10.1007/s00253-009-2377-x. [PubMed: 20135119]

(20). Morris TW; Reed KE; Cronan JE Lipoic Acid Metabolism in Escherichia Coli: The LplA and LipB Genes Define Redundant Pathways for Ligation of Lipoyl Groups to Apoprotein. J. Bacteriol 1995, 177 (1), 1–10. 10.1128/jb.177.1.1-10.1995. [PubMed: 8002607]

(21). Parsek MR; Val DL; Hanzelka BL; Cronan JE; Greenberg EP Acyl Homoserine-Lactone Quorum-Sensing Signal Generation. Proc. Natl. Acad. Sci. U. S. A 1999, 96 (8), 4360–4365. [PubMed: 10200267]

(22). Homma JY; Matsuura M; Kanegasaki S; Kawakubo Y; Kojima Y; Shibukawa N; Kumazawa Y; Yamamoto A; Tanamoto K; Yasuda T Structural Requirements of Lipid A Responsible for the Functions: A Study with Chemically Synthesized Lipid A and Its Analogues. J. Biochem. (Tokyo) 1985, 98 (2), 395–406. 10.1093/oxfordjournals.jbchem.a135294. [PubMed: 4066647]

(23). Beld J; Cang H; Burkart MD Visualizing the Chain-Flipping Mechanism in Fatty-Acid Biosynthesis. Angew. Chem. Int. Ed Engl 2014, 53 (52), 14456–14461. 10.1002/anie.201408576. [PubMed: 25354391]

(24). Cronan JE The Chain-Flipping Mechanism of ACP (Acyl Carrier Protein)-Dependent Enzymes Appears Universal. Biochem. J 2014, 460 (2), 157–163. 10.1042/BJ20140239. [PubMed: 24825445]

(25). Milligan JC; Lee DJ; Jackson DR; Schaub AJ; Beld J; Barajas JF; Hale JJ; Luo R; Burkart MD; Tsai S-C Molecular Basis for Interactions between an Acyl Carrier Protein and a Ketosynthase. Nat. Chem. Biol 2019, 15 (7), 669–671. 10.1038/s41589-019-0301-y. [PubMed: 31209348]

(26). Nguyen C; Haushalter RW; Lee DJ; Markwick PRL; Bruegger J; Caldara-Festin G; Finzel K; Jackson DR; Ishikawa F; O'Dowd B; McCammon JA; Opella SJ; Tsai S-C; Burkart MD Trapping the Dynamic Acyl Carrier Protein in Fatty Acid Biosynthesis. Nature 2014, 505 (7483), 427–431. 10.1038/nature12810. [PubMed: 24362570]

(27). Płoskoń E; Arthur CJ; Kanari ALP; Wattana-amorn P; Williams C; Crosby J; Simpson TJ; Willis CL; Crump MP Recognition of Intermediate Functionality by Acyl Carrier Protein over a Complete Cycle of Fatty Acid Biosynthesis. Chem. Biol 2010, 17 (7), 776–785. 10.1016/j.chembiol.2010.05.024. [PubMed: 20659690]

(28). Sztain T; Patel A; Lee DJ; Davis TD; McCammon JA; Burkart MD Modifying the Thioester Linkage Affects the Structure of the Acyl Carrier Protein. Angew. Chem. Int. Ed 2019, 58 (32), 10888–10892. 10.1002/anie.201903815.

(29). Xiao X; Yu X; Khosla C Metabolic Flux Between Unsaturated and Saturated Fatty Acids Is Controlled by the FabA:FabB Ratio in the Fully Reconstituted Fatty Acid Biosynthetic Pathway of E. Coli. Biochemistry 2013, 52 (46). 10.1021/bi401116n.

(30). Rock CO; Tsay JT; Heath R; Jackowski S Increased Unsaturated Fatty Acid Production Associated with a Suppressor of the FabA6(Ts) Mutation in Escherichia Coli. J. Bacteriol 1996, 178 (18), 5382–5387. 10.1128/jb.178.18.5382-5387.1996. [PubMed: 8808925]

(31). Finzel K; Nguyen C; Jackson DR; Gupta A; Tsai S-C; Burkart MD Probing the Substrate Specificity and Protein-Protein Interactions of the E. Coli Fatty Acid Dehydratase, FabA. Chem. Biol 2015, 22 (11), 1453–1460. 10.1016/j.chembiol.2015.09.009. [PubMed: 26526101]

(32). Dodge GJ; Patel A; Jaremko KL; McCammon JA; Smith JL; Burkart MD Structural and Dynamical Rationale for Fatty Acid Unsaturation in Escherichia Coli. Proc. Natl. Acad. Sci 2019, 116 (14), 6775–6783. 10.1073/pnas.1818686116. [PubMed: 30872475]

(33). S. Worthington A; D. Burkart M One-Pot Chemo-Enzymatic Synthesis of Reporter-Modified Proteins. Org. Biomol. Chem 2006, 4 (1), 44–46. 10.1039/B512735A. [PubMed: 16357994]

(34). Williamson MP Using Chemical Shift Perturbation to Characterise Ligand Binding. Prog. Nucl. Magn. Reson. Spectrosc 2013, 73, 1–16. 10.1016/j.pnmrs.2013.02.001. [PubMed: 23962882]

Author Manuscript Author Manuscript Author Manuscript Author Manuscript

(35). Waudby CA; Ramos A; Cabrita LD; Christodoulou J Two-Dimensional NMR Lineshape Analysis. Sci. Rep 2016, 6, 24826. 10.1038/srep24826. [PubMed: 27109776]

(36). Abagyan R; Totrov M Biased Probability Monte Carlo Conformational Searches and Electrostatic Calculations for Peptides and Proteins. J. Mol. Biol 1994, 235 (3), 983–1002. 10.1006/jmbi.1994.1052. [PubMed: 8289329]

(37). ICM—A new method for protein modeling and design: Applications to docking and structure prediction from the distorted native conformation - Abagyan - 1994 - Journal of Computational Chemistry - Wiley Online Library https://onlinelibrary.wiley.com/doi/abs/10.1002/jcc.540150503 (accessed Aug 31, 2020).

(38). Neves MAC; Totrov M; Abagyan R Docking and Scoring with ICM: The Benchmarking Results and Strategies for Improvement. J. Comput. Aided Mol. Des 2012, 26 (6), 675–686. 10.1007/s10822-012-9547-0. [PubMed: 22569591]

(39). Bartholow TG; Sztain T; Lee DJ; Abagyan R; Burkart MD Elucidation of Transient Protein-Protein Interactions within Carrier Protein-Dependent Biosynthesis. Commun. Biol. Accept

(40). Leesong M; Henderson BS; Gillig JR; Schwab JM; Smith JL Structure of a Dehydratase–Isomerase from the Bacterial Pathway for Biosynthesis of Unsaturated Fatty Acids: Two Catalytic Activities in One Active Site. Structure 1996, 4 (3), 253–264. 10.1016/S0969-2126(96)00030-5. [PubMed: 8805534]

(41). Andrec M; Hill RB; Prestegard JH Amide Exchange Rates in Escherichia Coli Acyl Carrier Protein: Correlation with Protein Structure and Dynamics. Protein Sci. 1995, 4 (5), 983–993. 10.1002/pro.5560040518. [PubMed: 7663354]

(42). Kozakov D; Li K; Hall DR; Beglov D; Zheng J; Vakili P; Schueler-Furman O; Paschalidis IC; Clore GM; Vajda S Encounter Complexes and Dimensionality Reduction in Protein–Protein Association. eLife 2014, 3, e01370. 10.7554/eLife.01370. [PubMed: 24714491]

(43). Shen Y; Paschalidis IC; Vakili P; Vajda S Protein Docking by the Underestimation of Free Energy Funnels in the Space of Encounter Complexes. PLOS Comput. Biol 2008, 4 (10), e1000191. 10.1371/journal.pcbi.1000191. [PubMed: 18846200]

(44). Colizzi F; Masetti M; Recanatini M; Cavalli A Atomic-Level Characterization of the Chain-Flipping Mechanism in Fatty-Acids Biosynthesis. J. Phys. Chem. Lett 2016, 7 (15), 2899–2904. 10.1021/acs.jpclett.6b01230. [PubMed: 27409360]

(45). Miyanaga A; Ouchi R; Ishikawa F; Goto E; Tanabe G; Kudo F; Eguchi T Structural Basis of Protein-Protein Interactions between a Trans-Acting Acyltransferase and Acyl Carrier Protein in Polyketide Disorazole Biosynthesis. J. Am. Chem. Soc 2018, 140 (25), 7970–7978. 10.1021/jacs.8b04162. [PubMed: 29870659]

(46). Misson LE; Mindrebo JT; Davis TD; Patel A; McCammon JA; Noel JP; Burkart MD Interfacial Plasticity Facilitates High Reaction Rate of E. Coli FAS Malonyl-CoA:ACP Transacylase, FabD. Proc. Natl. Acad. Sci 2020, 117 (39), 24224–24233. 10.1073/pnas.2009805117. [PubMed: 32929027]

(47). Mindrebo JT; Patel A; Kim WE; Davis TD; Chen A; Bartholow TG; La Clair JJ; McCammon JA; Noel JP; Burkart MD Gating Mechanism of Elongating β-Ketoacyl-ACP Synthases. Nat. Commun 2020, 11 (1), 1727. 10.1038/s41467-020-15455-x. [PubMed: 32265440]

Author Manuscript Author Manuscript Author Manuscript Author Manuscript

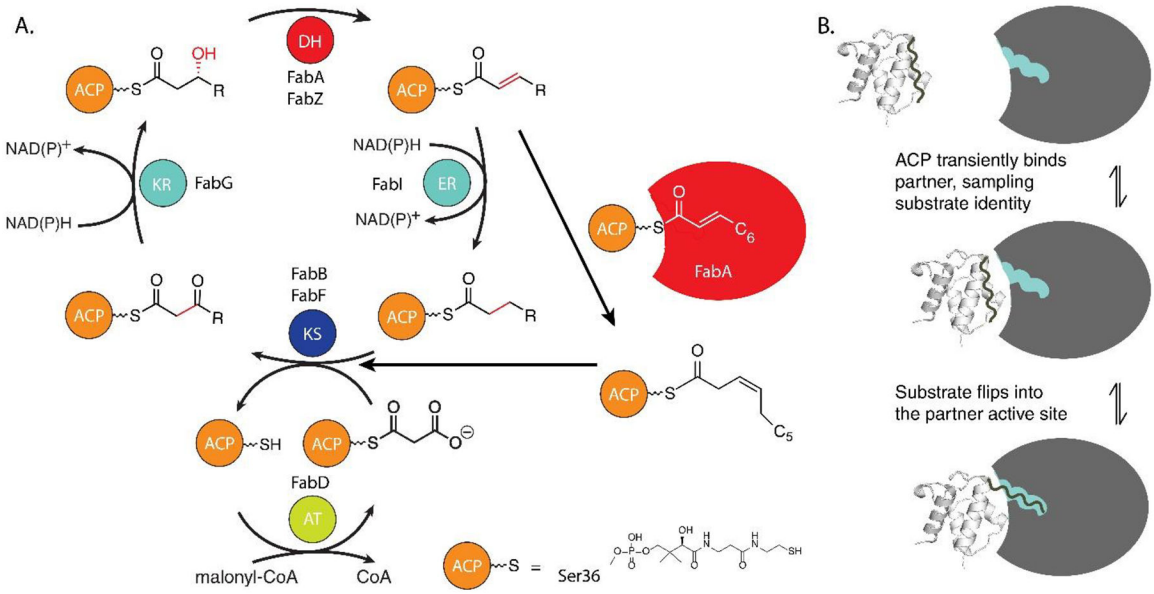

Figure 1.

A) The type II fatty acid biosynthesis cycle in *E. coli*. KS: ketosynthase, KR: Ketoreductase, DH: Dehydratase, ER: enoylreductase, TE: Thioesterase, AT: acyltransferase. The secondary role of FabA as an isomerase is specific to C10 acyl chains. B) AcpP as a 3 step process, wherein transient binding and unbinding can be performed separate from the chain flipping of substrates into a partner protein.

Author Manuscript Author Manuscript Author Manuscript Author Manuscript

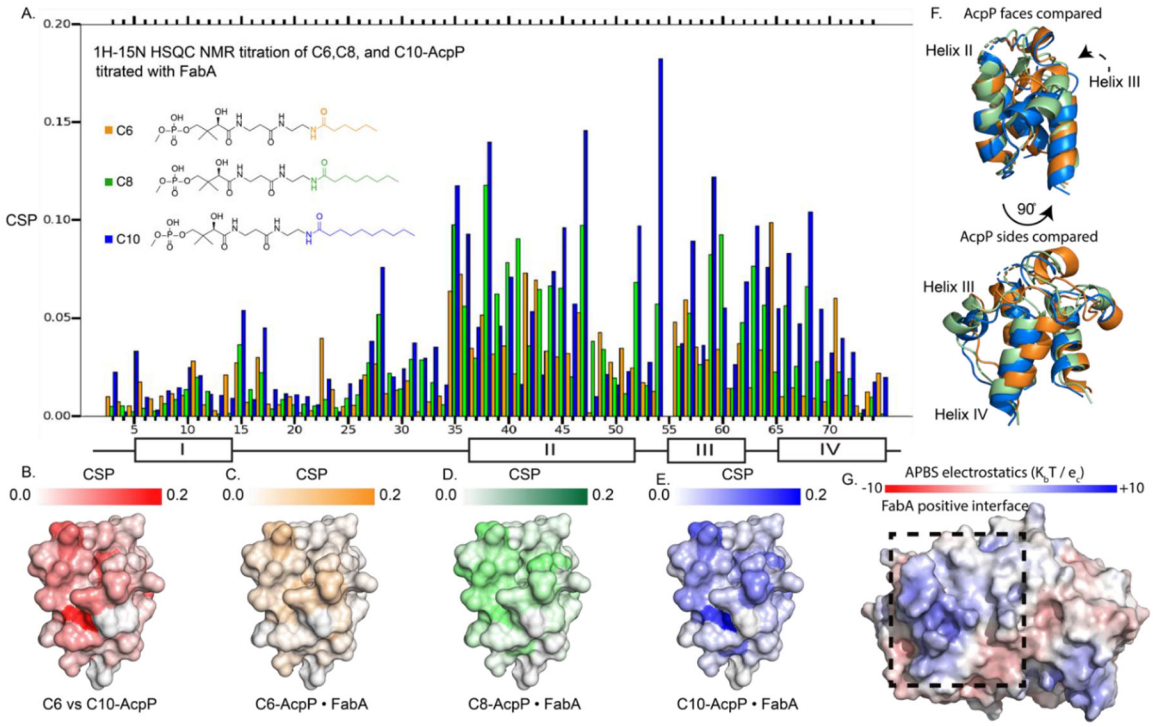

Figure 2.

A) The chemical shift perturbations (CSPs) of C6, C8, and C10 after titration to saturation with FabA. Each titration was performed to at least 1.5 molar equivalents of FabA. Individual perturbation graphs and spectra are presented in SI figures 1–4. B) The difference in residues between the C6 and C10-AcpP. C) The effect of FabA titration on the C6-AcpP D) The effect of FabA titration the C8-AcpP E) The effect of FabA titration C10-AcpP F) The starting MD derived structures of AcpP overlaid. Helix III exhibits the largest structural change between the chain lengths. G) The APBS electrostatics of the highly positive binding patch of FabA and negative face of AcpP. The left portion of the highlighted region is responsible for the majority of the binding interactions, binding helix III of AcpP.

Author Manuscript Author Manuscript Author Manuscript Author Manuscript

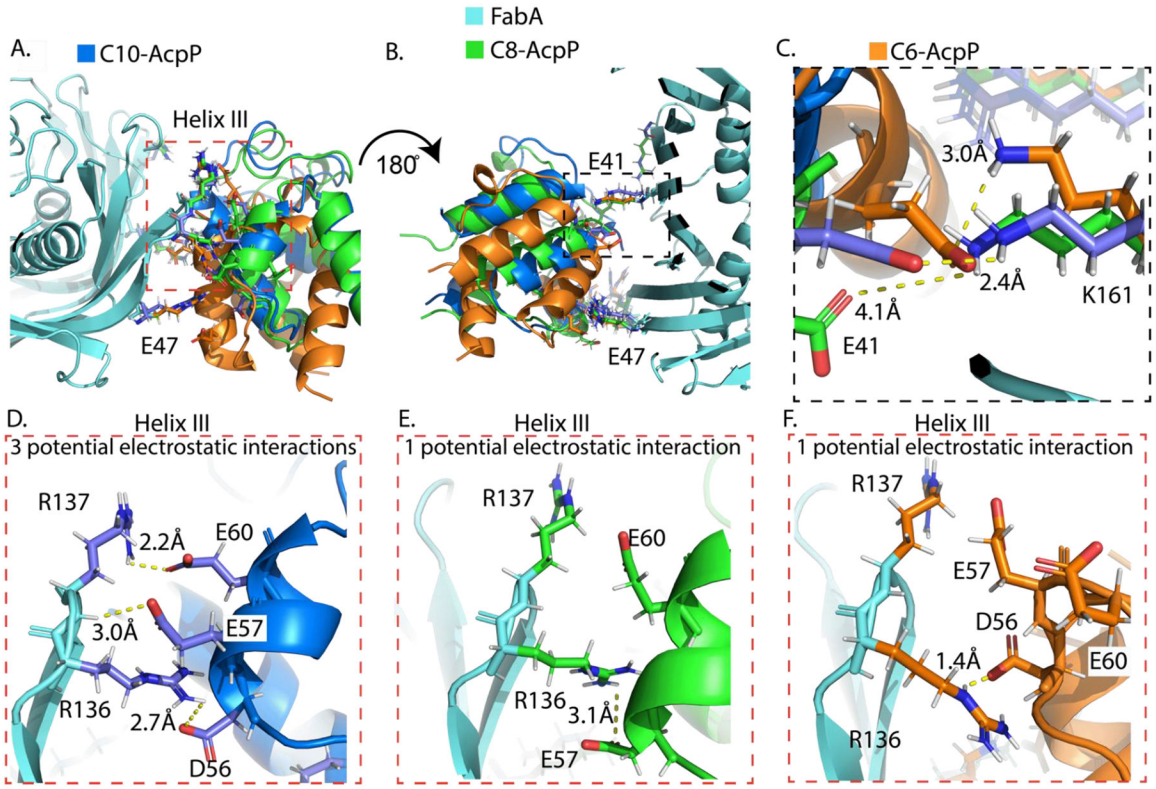

Figure 3.

A) The left face of the AcpP • FabA interaction. The helix III interactions are highlighted and focused on in panels D, E, and F. B) The right face of the AcpP • FabA interaction. E41 is highlighted and focused on in panel C. C) The interactions of E41 with K161' in C6, C8, and C10-AcpP. D) The interactions of helix III of C10-AcpP with FabA. Displaying the geometric complementarity of the C10-AcpP for the FabA residues E) The interactions of helix III of C8-AcpP with FabA. Displaying the non-complementarity of the binding region for the C8-AcpP helix III. F) The interactions of helix III of C6-AcpP with FabA. C6-AcpP has a helix III angled up and away from the region, such that only D56 at the base of helix III can form any interaction.

Author Manuscript Author Manuscript Author Manuscript Author Manuscript

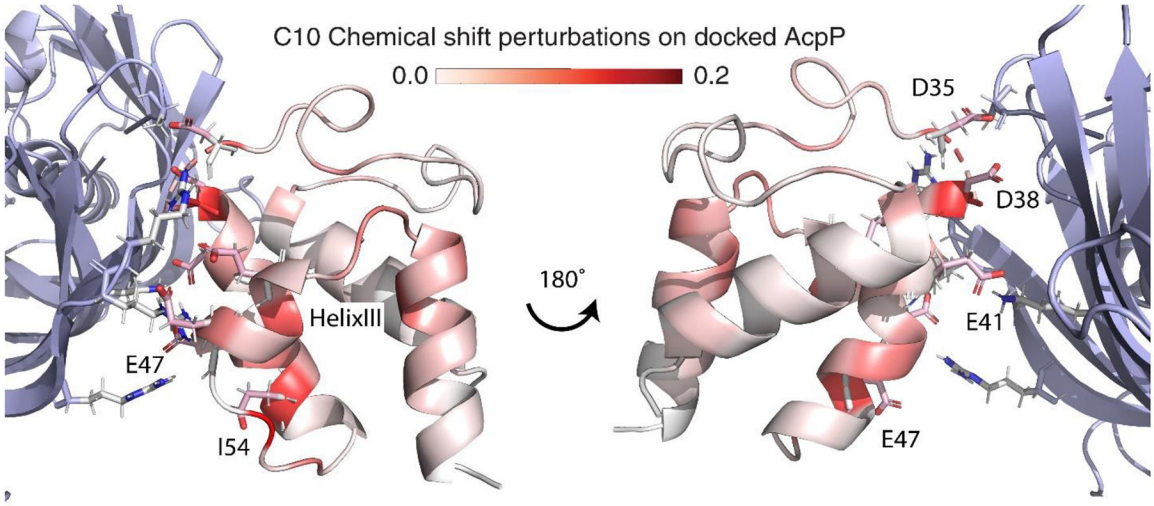

Figure 4.

The poses of C10-AcpP mapped onto the AcpP-FabA model. These residues are in agreement and further highlight the importance of I54, which most likely pushes the cargo out during chain flipping. Also, the importance of D35 and D38 in binding the poorly resolved loop region is shown in the CSPs, though not possible in the model.

Author Manuscript Author Manuscript Author Manuscript Author Manuscript

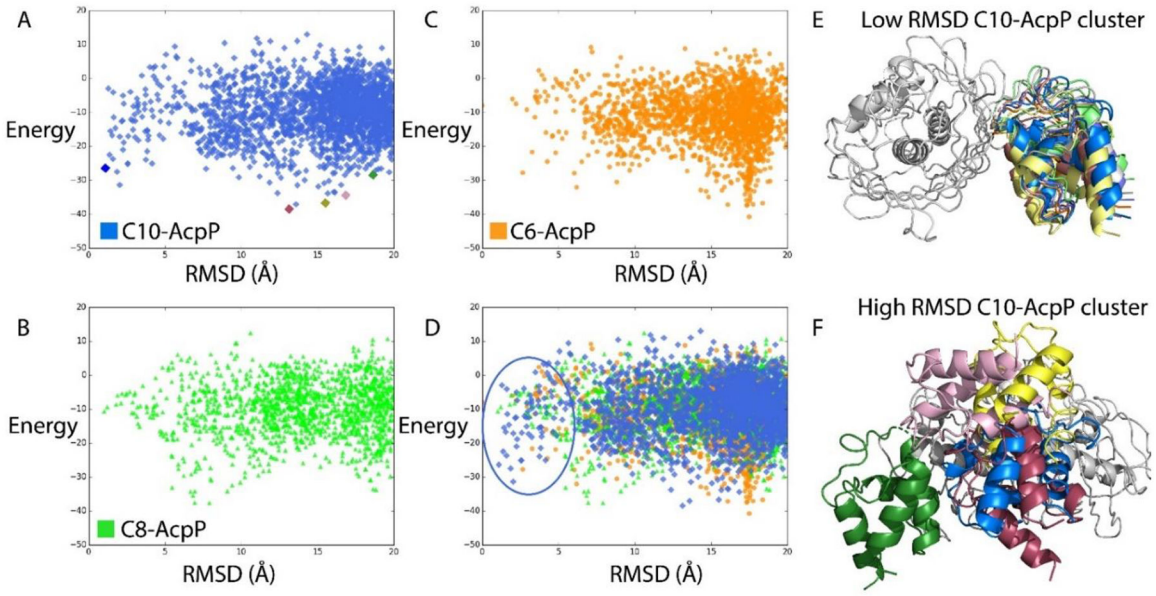

Figure 5.

A) The ensemble of conformations around the C10-AcpP • FabA interface. A narrowed RMSD range is presented in figure S7. Specific conformations at high RMSD are color coded blue, maroon, green, yellow, and pink panel F. B) The ensemble of conformations around the C8-AcpP • FabA interface. The conformations are presented in further detail in figure S8. C) The ensemble of conformations around the C6-AcpP • FabA interface. The conformations are presented in further detail in figure S8. D) An overlay of the conformations of the C6, C8, and C10-AcpP• FabA interface. The low RMSD displayed in panel E are circled in blue. E) The ensemble of low RMSD states of the C10-AcpP • FabA interface. F) A sample of low energy states of the C10-AcpP • FabA interface. Colors are matched to the model in panel A

Author Manuscript Author Manuscript Author Manuscript Author Manuscript

Table 1.

The average CSPs, TITAN analysis, and docking energetics of the AcpP • FabA interaction.

Chain Length	Average CSP	K_d (μM)	k_{off} (s^{-1})	Electrostatics (kcal/mol)	Van der Waal's (kcal/mol)	Total energy (kcal/mol)
C6	0.0241	34.8±5.9	311±64	−6.936	−11.18	−2.512
C8	0.0319	–	–	−5.149	−16.11	−11.79
C10	0.0434	8.6±3.0	4535±647	−8.065	−28.13	−22.36

Biochemistry. Author manuscript; available in PMC 2023 April 05.